Applied Physics Letters

Interferometric two-photon-absorption spectroscopy with three entangled photons

Cite as: Appl. Phys. Lett. **116**, 174003 (2020); https://doi.org/10.1063/5.0004617
Submitted: 12 February 2020 . Accepted: 12 April 2020 . Published Online: 29 April 2020

Lyuzhou Ye, and Shaul Mukamel

COLLECTIONS

Paper published as part of the special topic on Quantum Sensing with Correlated Light Sources
Note: This paper is part of the APL Special Collection on Quantum Sensing with Correlated Light Sources

Applied Physics Letters ARTICLE scitation.org/journal/apl

Interferometric two-photon-absorption spectroscopy with three entangled photons

Cite as: Appl. Phys. Lett. **116**, 174003 (2020); doi: 10.1063/5.0004617
Submitted: 12 February 2020 · Accepted: 12 April 2020 ·
Published Online: 29 April 2020

View Online Export Citation CrossMark

Lyuzhou Ye[a)] and Shaul Mukamel[b)]

AFFILIATIONS

Department of Chemistry and Department of Physics and Astronomy, University of California, Irvine, California 92697, USA

Note: This paper is part of the APL Special Collection on Quantum Sensing with Correlated Light Sources
[a)]**Electronic mail:** lyuzhouy@uci.edu
[b)]**Author to whom correspondence should be addressed:** smukamel@uci.edu

ABSTRACT

We propose an interferometric pump-probe technique that employs three entangled photons generated by cascaded spontaneous parametric downconversion. A Mach–Zehnder interferometer made of two three-port waveguide arrays is inserted in the optical path. Two independent phases introduced to manipulate the entangled photon state serve as control parameters and can selectively excite matter pathways. Compared to two-photon-absorption of an entangled photon-pair, the three-photon signals are significantly enhanced by frequency-dispersed photon-counting detection.

Quantum light can induce novel nonlinear optical processes, which are not possible with classical light.[1,2] One notable hallmark of quantum light is entanglement. The most common technique for generating entangled photons is spontaneous parametric downconversion of an input pump laser beam. Energy and momentum (phase matching) conservation gives rise to strong correlations between the generated photons. Entangled photon-pairs (biphotons) have been widely utilized in linear biphoton spectroscopy,[3–5] pump-probe spectroscopy,[6–9] and quantum imaging.[10–12] However, entangled three-photon (also known as triphoton or photon triplets) states in quantum spectroscopy have not been reported yet. The time-energy entanglement of triphoton states demonstrated in recent experiments[13–15] offers useful control parameters for quantum optical signals.

In this paper, we simulate frequency-dispersed photon-counting third-order two-photon absorption (TPA) spectroscopy signals from a three-level model system. The control parameters in classical pump-probe experiments are the pump frequency and the pump-probe time delay. In recent simulations of pump-probe spectroscopy with entangled photon pairs,[8,9,16] the central frequency of input laser pulses generating the biphoton state was scanned and the probe photon was spectrally dispersed. In Ref. 6, it was shown that nonlinear signals with two entangled photons can be manipulated by including a Mach–Zehnder interferometer (MZI) in the optical path to control the degree of entanglement. Using a triphoton state, Mährlein *et al.* proposed the complete three-photon Hong–Ou–Mandel (HOM) interference in a three-port waveguide array (WGA),[17] which is an extension of the celebrated two-photon HOM interference on a two-port beam splitter (BS).[18] Here, we utilize a MZI with two three-port WGAs to regulate the triphoton state by varying the phases of the two interferometer arms. We show that valuable information about excitation pathways in matter can be revealed using this setup via coincidence photon-counting of the spectrally dispersed probe and idler photons, compared to scanning the central frequency of input laser pulses. The TPA signal with three entangled photons is much stronger than that obtained with entangled photon pairs. Various matter excitation pathways can be enhanced or suppressed by properly choosing the phases introduced in the optical path by the three-port MZI.

We consider the triphoton state generated by cascaded spontaneous parametric downconversion (C-SPDC),[13–15] as sketched in Fig. 1(a). An input laser pulse with frequency ω_p passes through the nonlinear crystal to generate a pair of entangled photons (a_1 and a_a). The a_a photon then serves as a pump for a second SPDC process that creates a new pair of entangled photons (a_2 and a_3). In each SPDC, a pair of orthogonally polarized photons (a_1 and a_a for SPDC I and a_2 and a_3 for SPDC II) can be separated by a polarizing beam splitter (not shown in Fig. 1) after the SPDC. The details of the experimental setup can be found in Refs. 13 and 14. We assume that the input laser pulse and all output beams (1, a, 2, and 3) are collinear and propagate along z. At low input pulse intensity, the triphoton state is given by[14,19] [see Sec. S1 for details]

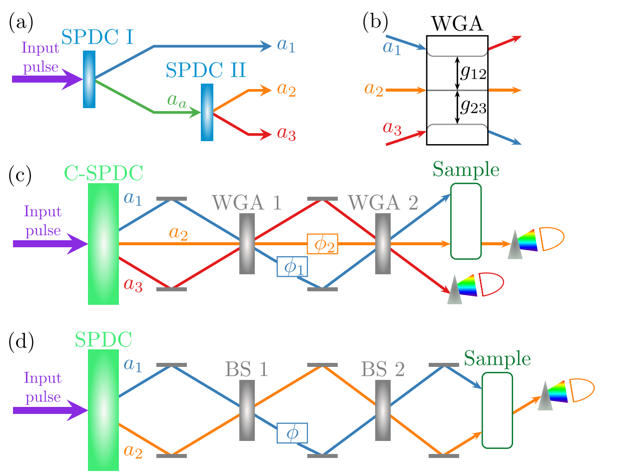

FIG. 1. (a) Triphoton state generation by cascaded SPDC. (b) The three-port WGA. g_{12} (g_{23}) are the couplings between modes 1 and 2 (2 and 3). Modes 1 and 3 are not coupled, i.e., $g_{31} = 0$. (c) The Interferometric pump-probe setup with three entangled photons (a_1, a_2, and a_3). The MZI is made out of two three-port WGAs. The two phases ϕ_1 and ϕ_2 are used to control the triphoton state. (d) Interferometric pump-probe setup with two entangled photons (a_1 and a_2). The MZI is made out of two beam splitters. A phase ϕ is introduced.

$$|\psi\rangle = \int\int\int d\omega_3 d\omega_2 d\omega_1\, \alpha_p F(\omega_1,\omega_2,\omega_3) a_3^\dagger(\omega_3) a_2^\dagger(\omega_2) a_1^\dagger(\omega_1)|0\rangle, \tag{1}$$

with the spectral amplitude ($\Omega_\mu = \omega_\mu - \omega_{\mu 0}$)

$$\begin{aligned} F(\omega_1,\omega_2,\omega_3) &= N \exp\left[-\gamma(T_{p1}\Omega_1 + T_{pa}\Omega_2 + T_{pa}\Omega_3)^2\right] \\ &\quad \times \exp\left[-\frac{(\Omega_1+\Omega_2+\Omega_3)^2}{2\sigma_p^2}\right] \\ &\quad \times \exp\left[-\gamma(T_{a2}\Omega_2 + T_{a3}\Omega_3)^2\right]. \end{aligned} \tag{2}$$

Here, $N = \left(\frac{1}{\pi\sigma_p^2}\right)^{1/4}\sqrt{\frac{2\gamma}{\pi}|T_{p1} - T_{pa}||T_{a2} - T_{a3}|}$ is a normalization constant. We have introduced four time-delay parameters $T_{\mu\nu} = L\left(\frac{1}{v_\mu} - \frac{1}{v_\nu}\right)$, where L is the nonlinear crystal length along z and $v_\mu = \frac{\partial k_{\mu z}}{\partial \omega_\mu}\Big|_{\omega_\mu = \omega_{\mu 0}}$ is the group velocity at frequency $\omega_{\mu 0}$.[1]

To measure the proposed signals, we add a Mach–Zehnder interferometer in the optical path. The MZI for the three-entangled-photon setup is made of two three-port WGAs. Figure 1(b) shows the WGA, which consists of three parallel single-mode-coupled waveguides.[20] The coupling of the 2D waveguides can be tuned by varying their distances.[21] Outer modes 1 and 3 are coupled to inner mode 2 but not to each other,[22] i.e., $g_{31} = 0$ in Fig. 1(b), because g_{31} is much smaller than the coupling between neighboring waveguides (g_{12} and g_{23}) and is neglected.[23] To determine the transformation matrix for the WGA, we consider a three-photon HOM effect.[17] This is an extension of the two-photon HOM effect[18] to the three-photon case, where the probability of detecting one photon in each output port of the WGA is zero. Details of the three-port WGA can be found in Sec. S2 of the supplementary material. Here, we present the final form of the transformation matrix for the WGA,

$$M = \begin{pmatrix} \frac{1}{2} & \frac{i}{\sqrt{2}} & -\frac{1}{2} \\ \frac{i}{\sqrt{2}} & 0 & \frac{i}{\sqrt{2}} \\ -\frac{1}{2} & \frac{i}{\sqrt{2}} & \frac{1}{2} \end{pmatrix}. \tag{3}$$

Figure 1(c) schematically depicts the interferometric pump-probe spectroscopy setup involving the entangled triphoton state. The three entangled photons generated by the C-SPDC pass through the three-port MZI (WGA 1 and WGA 2). Two phases ϕ_1 and ϕ_2 are introduced to control the triphoton state. The transformation matrix for the three-port MZI is $C = M^\dagger P M$. Here, $P = \mathrm{diag}(e^{i\phi_1}, e^{i\phi_2}, 1)$ describes the effect of interferometer phases on the triphoton state. M and $M^\dagger$ are the transformation matrices for the first and second WGAs, respectively.

After passing through the three-port MZI, the a_1 photon excites the molecule, which is then probed by the second photon a_2. The third photon a_3 (idler), which does not interact with the sample, is finally detected in coincidence with a_2. The spectrally dispersed two-photon counting signal is given by

$$\begin{aligned} S(\omega_2,\omega_3;\Gamma) &= \mathrm{tr}\left[a_3^\dagger(\omega_3)a_2^\dagger(\omega_2)a_2(\omega_2)a_3(\omega_3)\rho_{\mathrm{int}}(t\to\infty)\right], & (4)\\ &= \langle a_3^\dagger(\omega_3)a_2^\dagger(\omega_2)a_2(\omega_2)a_3(\omega_3)\rangle. & (5) \end{aligned}$$

Here, Γ denotes the set of control parameters, such as the entanglement times and the interferometer phases. In Eq. (4), we have taken the trace with respect to the joint field plus molecule density matrix in the interaction picture,

$$\rho_{\mathrm{int}}(t\to\infty) = \rho_{\mathrm{int}}(-\infty) - \mathscr{T}\left[\frac{i}{\hbar}\int_{-\infty}^{\infty} dt\, H_{\mathrm{int},-}(t)\rho_{\mathrm{int}}(t)\right], \tag{6}$$

where $\mathscr{T}$ represents the superoperator time-ordering, and the superoperator $H_{\mathrm{int},-}$ is defined by $H_{\mathrm{int},-}O = H_{\mathrm{int}}O - OH_{\mathrm{int}}$. The signal Eq. (5) can be further recast as (see Sec. S3A of the supplementary material)

$$S(\omega_2,\omega_3;\Gamma) = \frac{1}{\pi\hbar}\mathscr{T}\Im\int_{-\infty}^{\infty} dt\, e^{i\omega_2 t}\langle a_3^\dagger(\omega_3)a_3(\omega_3)E_2^\dagger(\omega_2)V(t)\rangle. \tag{7}$$

Here, V is the positive frequency part of the dipole operator, and $E_2^\dagger(\omega)$ is the Fourier transform of the photon field $E_2(t) = i\int d\omega\sqrt{\frac{\hbar}{4\pi\epsilon_0 cA}}a_2(\omega)e^{-i\omega t}$.

We have simulated the signal for the three-level model system shown in Fig. 2(a). All transition dipole moments are identical, i.e., $\mu_{ge} = \mu_{ef}$ ($e = \{e_1, e_2\}$ and $f = \{f_1, f_2\}$). The pump-probe signal is obtained by expanding the density matrix $\rho_{\mathrm{int}}(t)$ in Eq. (7) to second order in E_1 and first order in E_2. We then obtain eight terms. Four contribute to a Raman process, where the corresponding matter correlation functions are of the form $\langle VV^\dagger VV^\dagger\rangle$ and will not be considered further. The other four represent the TPA excitation pathways and are depicted in Fig. 2(b). They are denoted as TPA pathways since the system passes through a two-exciton state during the process, which is described by the matter correlation function $\langle VVV^\dagger V^\dagger\rangle$. The triphoton TPA signal is given by (see Sec. SIII B of the supplementary material)

$$S^{(3p)}_{\mathrm{TPA}}(\omega_2,\omega_3;\Gamma) = \frac{\omega_{10}\omega_{20}}{\pi\hbar^4}\left(\frac{\hbar}{4\pi\epsilon_0 cA}\right)^2 \Im\int d\omega_a\int d\omega_b \times\langle a_3^\dagger(\omega_3)a_2^\dagger(\omega_2)a_1^\dagger(\omega_a)a_3(\omega_3)a_2(\omega_b) \times a_1(\omega_2+\omega_a-\omega_b)\rangle\times g(\omega_2,\omega_a,\omega_b). \tag{8}$$

Here, the matter information is imprinted in the signal via the auxiliary function

$$\begin{aligned} g(\omega_2,\omega_a,\omega_b) = \sum_{e,e',f}\Bigg[&\frac{\mu_{ge'}}{\omega_2-\omega_{e'g}+i\eta}\frac{\mu_{e'f}\mu^*_{ef}}{\omega_2+\omega_a-\omega_{fg}+i\eta} \\ &\times\frac{\mu^*_{ge}}{\omega_b-\omega_{eg}+i\eta}+\frac{\mu_{ge'}}{\omega_2-\omega_{e'g}+i\eta} \\ &\times\frac{\mu_{e'f}\mu^*_{ef}}{\omega_2+\omega_a-\omega_{fg}+i\eta}\frac{\mu^*_{ge}}{\omega_2+\omega_a-\omega_b-\omega_{eg}+i\eta} \\ &-\frac{\mu_{ge'}}{-\omega_a+\omega_{e'g}+i\eta}\frac{\mu_{e'f}\mu^*_{ef}}{\omega_2+\omega_a-\omega_{fg}+i\eta} \\ &\times\frac{\mu^*_{ge}}{\omega_2+\omega_a-\omega_b-\omega_{eg}+i\eta}-\frac{\mu_{ge'}}{-\omega_a+\omega_{e'g}+i\eta} \\ &\times\frac{\mu_{e'f}\mu^*_{ef}}{\omega_2+\omega_a-\omega_{fg}+i\eta}\frac{\mu^*_{ge}}{\omega_b-\omega_{eg}+i\eta}\Bigg]. \end{aligned} \tag{9}$$

The normally ordered frequency-domain field correlation function in Eq. (8) is given by Eq. (S39) in Sec. SIII B of the supplementary material.

We now compare the triphoton signal with its entangled photon-pair counterpart.[6,8] As sketched in Fig. 1(d), the a_1 photon excites the sample, and a_2 acts as the probe, which is then spectrally dispersed and detected after interacting with the molecular system. The MZI consists of two beam splitters, and a phase ϕ is introduced in one of the two arms. The TPA signal with two entangled photons is given by (see Sec. SIV B of the supplementary material)

$$S^{(2p)}_{\mathrm{TPA}}(\omega_{p0},\omega_2;\Gamma) = \frac{\omega_{10}\omega_{20}}{\pi\hbar^4}\left(\frac{\hbar}{4\pi\epsilon_0 cA}\right)^2 \Im\int d\omega_a\int d\omega_b \times\langle a_2^\dagger(\omega_2)a_1^\dagger(\omega_a)a_2(\omega_b) \times a_1(\omega_2+\omega_a-\omega_b)\rangle g(\omega_2,\omega_a,\omega_b). \tag{10}$$

$S^{(2p)}_{\mathrm{TPA}}$ contains the same matter information [see Eq. (9)] as $S^{(3p)}_{\mathrm{TPA}}$. However, the two signals depend on different field correlation functions. $S^{(2p)}_{\mathrm{TPA}}$ is detected in (ω_{p0},ω_2) space, implying that the central frequency of input laser pulses is scanned. $S^{(3p)}_{\mathrm{TPA}}$ is given by the coincidence detection of probe (a_2) and idler (a_3) photons, holding the central frequency of input pulses fixed. In experiment, the production rate of photon triplets was considered to be lower than that of photon pairs.[13–15] In this work, we assume that the production rate for photon triplets is equal to that for photon pairs, in order to compare the corresponding TPA signals on an equal footing. Possible approaches have been proposed to increase the production rate for photon triplets.[24,25]

We start with the TPA signals with the triphoton state, Eq. (8). The three photons generated by C-SPDC are assumed to be degenerate, with the following parameters: the input pulse bandwidth $\sigma_p = 200\,\mathrm{cm}^{-1}$, the time delays $T_{p1} = 5$ fs, $T_{pa} = 15$ fs, $T_{a2} = 5$ fs, $T_{a3} = 15$ fs, and the central frequencies $\omega_{p0} = 30\,000\,\mathrm{cm}^{-1}$ and $\omega_{10} = \omega_{20} = \omega_{30} = 10\,000\,\mathrm{cm}^{-1}$.

The spectrally-dispersed photons ω_2 and ω_3 are detected in coincidence, while the input pulse frequency is held fixed. Energy conservation implies $\omega_p = \omega_1+\omega_2+\omega_3$. ω_p and ω_3, thus, fix the sum of ω_1 and ω_2. As depicted in Fig. 3, ω_1 and ω_2 are strongly anti-correlated. The bandwidths of the a_1 and a_2 photons are broad enough to cover both single-exciton (e_1 and e_2) states. This makes it possible to extract information about the excitation pathways in matter, as shown below.

The top row of Figs. 4(a)–4(c) shows the frequency-dispersed photon-counting TPA signals with three entangled photons $S^{(3p)}_{\mathrm{TPA}}$ given by diagrams (I) and (II) in Fig. 2(b) and their sum. The two interferometer phases are set to $\phi_1 = \phi_2 = 0$, and the corresponding transformation matrix C is the identity. The narrow input pulse bandwidth σ_p selectively excites one of the two doubly excited f states. The resonances at $9500\,\mathrm{cm}^{-1}$ and $8500\,\mathrm{cm}^{-1}$ along ω_3 correspond to excitation of the f_2 and f_1 states [see Fig. 2(a)], respectively. Along the probe frequency ω_2, the resonances are at $10\,000\,\mathrm{cm}^{-1}$ and $11\,000\,\mathrm{cm}^{-1}$, implying that the ω_2 photon carries information about the $e_{1,2}\to g$ transitions, while in Fig. 4(b), the four resonances (from left to right) along ω_2 correspond to the $f_1\to e_2$, $f_1\to e_1$, $f_2\to e_2$, and $f_2\to e_1$ transitions. The sum of Figs. 4(a) and 4(b) is plotted in Fig. 4(c), where the eight resonances are labeled as A–H. We can, thus, clearly identify the excitation pathways by utilizing the photon-

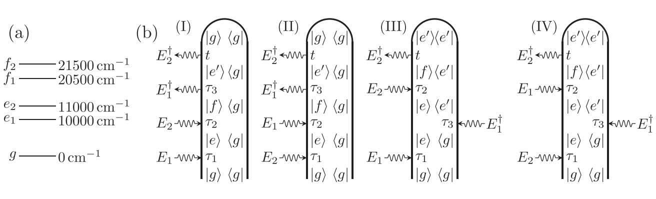

FIG. 2. (a) The three-level model system used in our simulations. The dipole moments of all transitions are taken to be the same i.e., $\mu_{ge} = \mu_{ef}$ ($e = \{e_1, e_2\}$ and $f = \{f_1, f_2\}$). (b) Loop diagrams (I)–(IV) for TPA pathways. Note that there is no time ordering control of the interactions between the left and right branches.

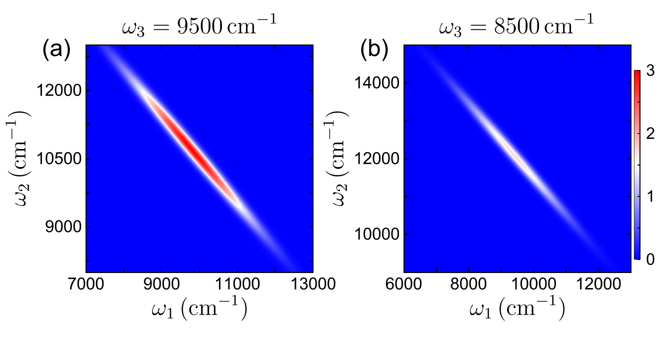

FIG. 3. Frequency correlations $|F(\omega_1,\omega_2,\omega_3)|^2$ [Eq. (2)] between the excitation (ω_1) and probe (ω_2) photons of the triphoton state when the frequency of the idler (ω_3) photon is held constant at (a) $\omega_3 = 9500\,\mathrm{cm}^{-1}$ and (b) $\omega_3 = 8500\,\mathrm{cm}^{-1}$. Other parameters are the input pulse bandwidth $\sigma_p = 200\,\mathrm{cm}^{-1}$, the time delays $T_{p1} = 5$ fs, $T_{pa} = 15$ fs, $T_{a2} = 5$ fs, $T_{a3} = 15$ fs, and the central frequencies $\omega_{p0} = 30\,000\,\mathrm{cm}^{-1}$ and $\omega_{10} = \omega_{20} = \omega_{30} = 10\,000\,\mathrm{cm}^{-1}$.

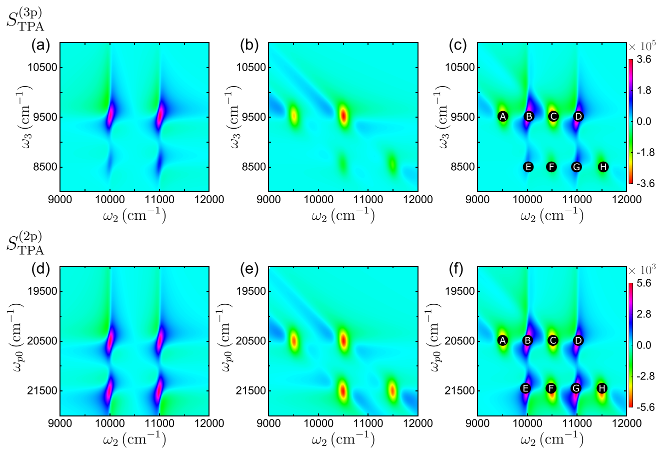

FIG. 4. Top row: Interferometric TPA signal with three entangled photons $S_{\mathrm{TPA}}^{(3p)}$, Eq. (8), with $\phi_1 = 0$ and $\phi_2 = 0$. (a) Contributions of diagrams (I) and (II) in Fig. 2. (b) Contributions of diagrams (III) and (IV). (c) The total signal [sum of (a) and (b)]. Points A–G represent the eight major resonances. Bottom Row: The same as the first row, but for the interferometric TPA signal with two entangled photons $S_{\mathrm{TPA}}^{(2p)}$, Eq. (10), with $\phi = 0$.

counting detection of the probe and idler photons in the frequency domain.

For comparison, the TPA signals generated by two entangled photons $S_{\mathrm{TPA}}^{(2p)}$ are depicted in the bottom row of Figs. 4(d)–4(f). The following parameters for the SPDC generated photon-pair were used: the input pulse bandwidth $\sigma_p = 200\,\mathrm{cm}^{-1}$, the time delays $T_{p1} = 5\,\mathrm{fs}$, $T_{p2} = 15\,\mathrm{fs}$, and the central frequencies $\omega_{10} = \omega_{20} = \omega_{p0}/2$, which are comparable to those used for $S_{\mathrm{TPA}}^{(3p)}$. The signal is plotted in (ω_{p0}, ω_2) space, where the central frequency of the input laser pulses is scanned and the probe photon a_2 is spectrally dispersed. The resonances along the ω_{p0}-axis directly reveal the two-exciton states f_1 and f_2. This is different from the $S_{\mathrm{TPA}}^{(3p)}$ signal, where the two-exciton resonances along ω_3 are obtained by the frequency difference $\omega_{p0} - \omega_3$ since we have fixed the central frequency of input pulses and dispersed the idler photon for the measurement of the $S_{\mathrm{TPA}}^{(3p)}$ signal.

The triphoton spectrally dispersed TPA signal $S_{\mathrm{TPA}}^{(3p)}$ provides the same information about the matter excitations as its biphoton counterpart $S_{\mathrm{TPA}}^{(2p)}$. However, the resonance strengths in Fig. 4(c) are 64 times higher than those in Fig. 4(f). We further note that in Fig. 4(c), the resonances at $\omega_3 = 9500\,\mathrm{cm}^{-1}$ (points A–D) are much stronger than those at $\omega_3 = 8500\,\mathrm{cm}^{-1}$ (points E–H), indicating that the f_1 state is more favorably excited. This is because, as can be seen in Fig. 3, the marginal distribution of the probe photon (ω_2) at $\omega_3 = 9500\,\mathrm{cm}^{-1}$ is stronger than that at $\omega_3 = 8500\,\mathrm{cm}^{-1}$. We, thus, have a higher probability to detect the a_2-photon at $\omega_3 = 9500\,\mathrm{cm}^{-1}$ than that at $\omega_3 = 8500\,\mathrm{cm}^{-1}$, making the corresponding resonances stronger. The eight resonances in the $S_{\mathrm{TPA}}^{(2p)}$ signal in Fig. 4(f) have, on the other hand, very similar strengths. Figure 5 displays the marginal distributions of the a_2-photon of the biphoton state. Since the probabilities of detecting the a_2-photon are very close for the two input pulse central frequencies $\omega_{p0} = 20\,500\,\mathrm{cm}^{-1}$ [Fig. 5(a)] and $21\,500\,\mathrm{cm}^{-1}$ [Fig. 5(b)], the corresponding resonance strengths are very similar.

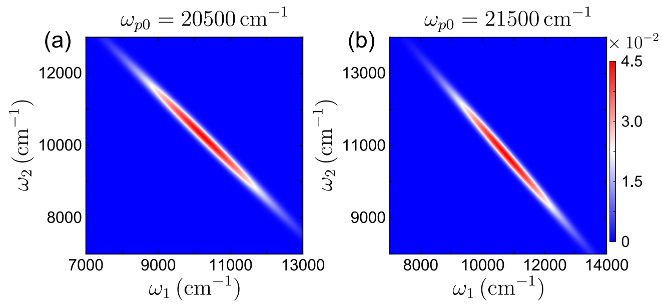

FIG. 5. Frequency correlations $|F(\omega_1, \omega_2)|^2$ [Eq. (S54) of the supplementary material] between the excitation (ω_1) and probe (ω_2) photons of the entangled photon-pair when the central frequency of input pulses is (a) $\omega_{p0} = 20\,500\,\mathrm{cm}^{-1}$ and (b) $\omega_{p0} = 21\,500\,\mathrm{cm}^{-1}$. The parameters used for the entangled photon-pair are the input pulse bandwidth $\sigma_p = 200\,\mathrm{cm}^{-1}$, the time delays $T_{p1} = 5\,\mathrm{fs}$, $T_{pa} = 15\,\mathrm{fs}$, $T_{p2} = 15\,\mathrm{fs}$, and the central frequencies $\omega_{10} = \omega_{20} = \omega_{p0}/2$.

The above signals reflect the interference of various excitation pathways of the field and matter. For a general interferometric setup, the field correlation function Eq. (S39) [or (S53)] also depends on the phase(s) introduced in the MZI. We next explore the possible manipulations of the doubly excited states (f_1 or f_2) by varying the phases of the MZI. Figure 6(a) shows the variation of the eight resonances [points A–H in Fig. 4(f)] of $S_{\mathrm{TPA}}^{(2p)}$ with the interferometer phase ϕ. Their strengths are virtually identical in any phase ϕ. Therefore, the phase ϕ introduced to the MZI for the entangled photon-pair cannot select the desired two-exciton state (f_1 or f_2). However, it is interesting that at $\phi = \pi/2$, the overall biphoton TPA signal $S_{\mathrm{TPA}}^{(2p)}$ is suppressed [$\sim 10^{-2}$, five orders of magnitude weaker than the signal in Fig. 4(f)]. Suppression of the TPA can be used to single out other signals.

Figure 6(b) shows the interferometric TPA signal $S_{\mathrm{TPA}}^{(3p)}$ with $\phi_1 = 0.62\pi$ and $\phi_2 = 0.32\pi$. Compared to Fig. 4(c), the $\omega_3 = 8500\,\mathrm{cm}^{-1}$ resonances are enhanced, while those at $\omega_3 = 9500\,\mathrm{cm}^{-1}$ are suppressed, indicating that the two-exciton state f_2 is efficiently excited.

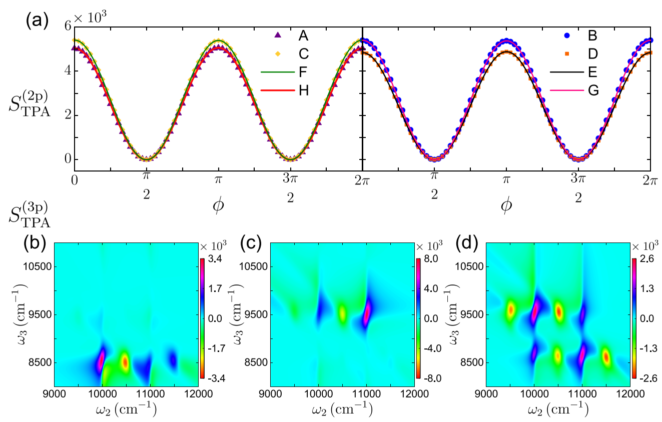

FIG. 6. (a) Variation of the absolute values of the eight resonances of signal $S_{\mathrm{TPA}}^{(2p)}$ in Fig. 4(f) with the interferometer phase ϕ. Triphoton signal $S_{\mathrm{TPA}}^{(3p)}$ with (b) $\phi_1 = 0.62\pi$ and $\phi_2 = 0.32\pi$, (c) $\phi_1 = 0.54\pi$ and $\phi_2 = 1.26\pi$, and (d) $\phi_1 = 1.86\pi$ and $\phi_2 = 0.42\pi$.

Furthermore, by adjusting the phases ϕ_1 and ϕ_2, we can also enhance the f_1 state and suppress the f_2 state [see Fig. 6(c)] or make their resonance strengths similar [see Fig. 6(d)]. Although the signals with the nonzero phases are weaker, they are still comparable to the biphoton TPA signal in Fig. 4(f). Thus, the two-exciton states can be manipulated by varying the two interferometer phases (ϕ_1 and ϕ_2) introduced in the triphoton state, which is not possible with an entangled photon-pair.

To conclude, we have proposed a pump-probe TPA technique that makes use of three entangled photons. The triphoton state is obtained by a cascaded spontaneous parametric downconversion process at low input pulse intensity, which helps avoid damage to delicate samples. Interferometric TPA signals can be manipulated by adding a three-port MZI in the optical path. The three entangled photons exhibit strong frequency correlations, and the triphoton signals $S^{(3p)}_{\mathrm{TPA}}$ [see Figs. 4(a)–4(c)] allow us to extract information about the TPA pathways of the matter system with the input laser pulse frequency being fixed. The spectrally dispersed photon-counting signal with the triphoton state is much stronger than the TPA signal with the biphoton state, due to the higher distribution probabilities of the detected photons of the triphoton state. The two interferometer phases offer an effective control tool for selecting the two-exciton pathways.

See the supplementary material for the derivations of the triphoton state generated by cascaded spontaneous parametric downconversion, derivations of the transformation matrix for the three-port waveguide array, and derivations of the two-photon-absorption signals.

This work was supported by National Science Foundation Grant No. CHE-1953045 and the Chemical Sciences, Geosciences, and Biosciences Division, Office of Basic Energy Sciences, Office of Science, U.S. Department of Energy Awards (DOE) No. DE-FG02-04ER15571. L.Y. was supported by the DOE grant.

REFERENCES

[1]K. E. Dorfman, F. Schlawin, and S. Mukamel, "Nonlinear optical signals and spectroscopy with quantum light," Rev. Mod. Phys. **88**, 045008 (2016).
[2]S. Mukamel, M. Freyberger, W. P. Schleich, M. Bellini, A. Zavatta, G. Leuchs, C. Silberhorn, R. W. Boyd, L. S. Soto, A. Stefanov *et al.*, "Roadmap on quantum light spectroscopy," J. Phys. B **53**, 072002 (2020).
[3]A. Yabushita and T. Kobayashi, "Spectroscopy by frequency-entangled photon pairs," Phys. Rev. A **69**, 013806 (2004).
[4]A. Kalachev, D. Kalashnikov, A. Kalinkin, T. Mitrofanova, A. Shkalikov, and V. Samartsev, "Biphoton spectroscopy in a strongly nondegenerate regime of SPDC," Laser Phys. Lett. **5**, 600–602 (2008).
[5]D. A. Kalashnikov, Z. Pan, A. I. Kuznetsov, and L. A. Krivitsky, "Quantum spectroscopy of plasmonic nanostructures," Phys. Rev. X **4**, 011049 (2014).
[6]O. Roslyak, C. A. Marx, and S. Mukamel, "Nonlinear spectroscopy with entangled photons: Manipulating quantum pathways of matter," Phys. Rev. A **79**, 033832 (2009).
[7]O. Roslyak and S. Mukamel, "Multidimensional pump-probe spectroscopy with entangled twin-photon states," Phys. Rev. A **79**, 063409 (2009).
[8]F. Schlawin and S. Mukamel, "Two-photon spectroscopy of excitons with entangled photons," J. Chem. Phys. **139**, 244110 (2013).
[9]F. Schlawin, K. E. Dorfman, and S. Mukamel, "Pump-probe spectroscopy using quantum light with two-photon coincidence detection," Phys. Rev. A **93**, 023807 (2016).
[10]R. S. Aspden, D. S. Tasca, R. W. Boyd, and M. J. Padgett, "Epr-based ghost imaging using a single-photon-sensitive camera," New J. Phys. **15**, 073032 (2013).
[11]G. B. Lemos, V. Borish, G. D. Cole, S. Ramelow, R. Lapkiewicz, and A. Zeilinger, "Quantum imaging with undetected photons," Nature **512**, 409 (2014).
[12]S. Asban, K. E. Dorfman, and S. Mukamel, "Quantum phase-sensitive diffraction and imaging using entangled photons," Proc. Natl. Acad. Sci. U. S. A. **116**, 11673–11678 (2019).
[13]H. Hübel, D. R. Hamel, A. Fedrizzi, S. Ramelow, K. J. Resch, and T. Jennewein, "Direct generation of photon triplets using cascaded photon-pair sources," Nature **466**, 601–603 (2010).
[14]L. K. Shalm, D. R. Hamel, Z. Yan, C. Simon, K. J. Resch, and T. Jennewein, "Three-photon energy-time entanglement," Nat. Phys. **9**, 19–22 (2013).
[15]D. R. Hamel, L. K. Shalm, H. Hübel, A. J. Miller, F. Marsili, V. B. Verma, R. P. Mirin, S. W. Nam, K. J. Resch, and T. Jennewein, "Direct generation of three-photon polarization entanglement," Nat. Photonics **8**, 801–807 (2014).
[16]F. Schlawin, K. E. Dorfman, B. P. Fingerhut, and S. Mukamel, "Manipulation of two-photon-induced fluorescence spectra of chromophore aggregates with entangled photons: A simulation study," Phys. Rev. A **86**, 023851 (2012).
[17]S. Mährlein, J. V. Zanthier, and G. S. Agarwal, "Complete three photon hong-ou-mandel interference at a three port device," Opt. Express **23**, 15833–15847 (2015).
[18]C. K. Hong, Z. Y. Ou, and L. Mandel, "Measurement of subpicosecond time intervals between two photons by interference," Phys. Rev. Lett. **59**, 2044–2046 (1987).
[19]Q.-Y. Zhang, G.-T. Xue, P. Xu, Y.-X. Gong, Z. Xie, and S. Zhu, "Manipulation of tripartite frequency correlation under extended phase matchings," Phys. Rev. A **97**, 022327 (2018).
[20]K. Suzuki, V. Sharma, J. G. Fujimoto, E. P. Ippen, and Y. Nasu, "Characterization of symmetric [3×3] directional couplers fabricated by direct writing with a femtosecond laser oscillator," Opt. Express **14**, 2335 (2006).
[21]S. Martellucci and A. N. Chester, *Integrated Optics: Physics and Applications* (Springer Science & Business Media, 1983), Vol. 91.
[22]B. E. A. Saleh and M. C. Teich, *Fundamentals of Photonics* (John Wiley & Sons, 2007).
[23]H. Ogiwara, "Optical waveguide 3×3 switch: Theory of tuning and control," Appl. Opt. **18**, 510–515 (1979).
[24]S. Richard, K. Bencheikh, B. Boulanger, and J. A. Levenson, "Semiclassical model of triple photons generation in optical fibers," Opt. Lett. **36**, 3000–3002 (2011).
[25]M. Corona, K. Garay-Palmett, and A. B. U'Ren, "Experimental proposal for the generation of entangled photon triplets by third-order spontaneous parametric downconversion in optical fibers," Opt. Lett. **36**, 190–192 (2011).

SUPPLEMENTARY MATERIAL:
Interferometric two-photon absorption spectroscopy with three entangled photons

Lyuzhou Ye* and Shaul Mukamel†

Department of Chemistry and Department of Physics and Astronomy,
University of California, Irvine, CA 92697, USA

(Dated: February 5, 2020)

S1. DERIVATION OF THE TRIPHOTON STATE

We assume the following form for the classical pump pulse envelope [see Fig. 1(a) of the main text]

$$E_p^{(+)}(\boldsymbol{r},t) = \int d\boldsymbol{q}_p \int d\omega_p\, G(\boldsymbol{q}_p)\alpha_p \mathscr{A}(\omega_p) e^{i\boldsymbol{q}_p\cdot\boldsymbol{\rho}} e^{ik_{pz}z} e^{-i\omega_p t}, \tag{S1}$$

where $\boldsymbol{q}_p$ and $\boldsymbol{\rho}$ are the transverse components of the wavevector and coordinate, respectively. $G(\boldsymbol{q}_p)$ and $\mathscr{A}(\omega_p)$ are the spatial and spectral envelopes, respectively. Generating a well-seperated triphton state requires a low pump intensity α_p. The photon field operator for mode $\mu = 1,2,3,a$ is expanded as [1]

$$E_\mu^{(+)}(\boldsymbol{r},t) = i\int d\boldsymbol{q}_\mu \int d\omega_\mu \sqrt{\frac{\hbar\omega_\mu}{2\varepsilon_0 n_\mu^2(\omega_\mu)}}\, a_\mu(\boldsymbol{q}_\mu,\omega_\mu) e^{i\boldsymbol{q}_\mu\cdot\boldsymbol{\rho}} e^{ik_{\mu z}z} e^{-i\omega_\mu t}. \tag{S2}$$

The two SPDC processes (I and II) are described by the effective interaction Hamiltonians

$$H_{\rm I}(t) = \int d\boldsymbol{r}_{\rm I}\, \chi_{\rm I}^{(2)} E_p^{(+)}(\boldsymbol{r}_{\rm I},t) E_1^{(-)}(\boldsymbol{r}_{\rm I},t) E_a^{(-)}(\boldsymbol{r}_{\rm I},t) + \text{H.c.}, \tag{S3}$$

$$H_{\rm II}(t) = \int d\boldsymbol{r}_{\rm II}\, \chi_{\rm II}^{(2)} E_a^{(+)}(\boldsymbol{r}_{\rm II},t) E_2^{(-)}(\boldsymbol{r}_{\rm II},t) E_3^{(-)}(\boldsymbol{r}_{\rm II},t) + \text{H.c.}. \tag{S4}$$

Here, the integrals are taken over their respective interaction volumes. $\chi_{\rm I}^{(2)}$ and $\chi_{\rm II}^{(2)}$ are the second-order susceptibilities of the nonlinear crystals for the first and second SPDC processes, respectively.

We assume that the pump and all output beams ($\mu = 1$, a, 2, and 3) are collinear and propagate along z, i.e., $\boldsymbol{k}_\mu = k_{\mu z}\hat{z}$. By applying the standard perturbation theory, the triphoton state is give by [1, 2]

$$\begin{aligned}|\psi\rangle =& \mathscr{C} \iiint d\omega_3 d\omega_2 d\omega_1\, \alpha_p \mathscr{A}(\omega_1+\omega_2+\omega_3) \text{sinc}\left[\frac{T_{a2}}{2}(\omega_2-\omega_{20}) + \frac{T_{a3}}{2}(\omega_3-\omega_{30})\right] \\ & \times \text{sinc}\left[\frac{T_{p1}}{2}(\omega_1-\omega_{10}) + \frac{T_{pa}}{2}(\omega_2-\omega_{20}+\omega_3-\omega_{30})\right] a_3^\dagger(\omega_3) a_2^\dagger(\omega_2) a_1^\dagger(\omega_1)\,|0\rangle\,. \end{aligned}\tag{S5}$$

* lyuzhouy@uci.edu

† smukamel@uci.edu

For computational convenience, we approximate the sinc-function by a Gaussian with the same width [3, 4]: $\mathrm{sinc}\,(x/2) \approx \exp\left(-\gamma x^2\right)$, with $\gamma = 0.0482304$. The triphoton state can be finally recast as

$$|\psi\rangle = \iiint d\omega_3 d\omega_2 d\omega_1\, \alpha_p F(\omega_1, \omega_2, \omega_3) a_3^\dagger(\omega_3) a_2^\dagger(\omega_2) a_1^\dagger(\omega_1)\, |0\rangle\,, \tag{S6}$$

where $F(\omega_1, \omega_2, \omega_3)$ is given by Eq. (2) of the main text.

S2. TRANSFORMATION MATRIX FOR THE THREE-PORT WAVEGUIDE ARRAY

We examine the three-photon interference at a three-port WGA. A generalization of the HOM effect to three indistinguishable photons was proposed in Ref. 5. A complete destructive interference of three photons can be observed in a three-port device which consists of three parallel single-mode-coupled waveguides [6], as sketched in Fig. 2(a). The three-photon interference is described by the effective Hamiltonian [5]

$$H = \hbar(g_{12} a_1^\dagger a_2 + g_{23} a_2^\dagger a_3) + \text{H.c.}. \tag{S7}$$

Here, a_1, a_2 and a_3 are annihilation operators of the input modes.

The time evolution of the modes is described by

$$\frac{d}{dt}A(t) \equiv \frac{d}{dt}\begin{pmatrix} a_1^\dagger(t) \\ a_2^\dagger(t) \\ a_3^\dagger(t) \end{pmatrix} = iM(t)A(t) \equiv i \begin{pmatrix} 0 & g_{12}^* & 0 \\ g_{12} & 0 & g_{23}^* \\ 0 & g_{23} & 0 \end{pmatrix} A(t), \tag{S8}$$

where we have defined $A(t) = (a_1^\dagger, a_2^\dagger, a_3^\dagger)^T$, and M is the coupling matrix. Solving this equation gives

$$A(t) = e^{iMt}A(0) = V(t)A(0), \tag{S9}$$

where, $V = e^{iMt}$ is the transformation matrix between the input and output modes.

We assume that the couplings g_{12} and g_{23} are real. The eigenvalues of matrix M are $\lambda_1 = 0$, $\lambda_2 = -\sqrt{g_{12}^2 + g_{23}^2}$, and $\lambda_3 = \sqrt{g_{12}^2 + g_{23}^2}$, and the corresponding eigenvectors are

$$v_1 = \left(-\frac{g_{23}}{\sqrt{g_{12}^2 + g_{23}^2}}, 0, \frac{g_{12}}{\sqrt{g_{12}^2 + g_{23}^2}} \right)^T, \tag{S10}$$

$$v_2 = \left(\frac{g_{12}}{\sqrt{2}\sqrt{g_{12}^2 + g_{23}^2}}, -\frac{1}{\sqrt{2}}, \frac{g_{23}}{\sqrt{2}\sqrt{g_{12}^2 + g_{23}^2}} \right)^T, \tag{S11}$$

$$v_3 = \left(\frac{g_{12}}{\sqrt{2}\sqrt{g_{12}^2 + g_{23}^2}}, \frac{1}{\sqrt{2}}, \frac{g_{23}}{\sqrt{2}\sqrt{g_{12}^2 + g_{23}^2}} \right)^T. \tag{S12}$$

The coupling matrix is

$$M = \begin{pmatrix} v_1 & v_2 & v_3 \end{pmatrix} \begin{pmatrix} 0 & 0 & 0 \\ 0 & -\sqrt{g_{12}^2+g_{23}^2} & 0 \\ 0 & 0 & \sqrt{g_{12}^2+g_{23}^2} \end{pmatrix} \begin{pmatrix} v_1^T \\ v_2^T \\ v_3^T \end{pmatrix}. \tag{S13}$$

The transformation matrix then reads

$$V = e^{iMt} = \begin{pmatrix} \sin^2\theta + \cos^2\theta\cos G & i\cos\theta\sin G & \cos\theta\sin\theta(\cos G - 1) \\ i\cos\theta\sin G & \cos G & i\sin\theta\sin G \\ \cos\theta\sin\theta(\cos G-1) & i\sin\theta\sin G & \cos^2\theta + \sin^2\theta\cos G \end{pmatrix}, \tag{S14}$$

where we have defined $G = \sqrt{g_{12}^2+g_{23}^2}t$, $\cos\theta = \frac{g_{12}}{\sqrt{g_{12}^2+g_{23}^2}}$, and $\sin\theta = \frac{g_{23}}{\sqrt{g_{12}^2+g_{23}^2}}$. The three-port WGA will transform the input modes ($i = 1,2,3$) as

$$a_i^\dagger \to V_{i1}a_1^\dagger + V_{i2}a_2^\dagger + V_{i3}a_3^\dagger. \tag{S15}$$

We consider the input state

$$|\psi_{\text{in}}\rangle = |1\rangle_1 |1\rangle_2 |1\rangle_3 = a_1^\dagger a_2^\dagger a_3^\dagger |0\rangle_1 |0\rangle_2 |0\rangle_3 . \tag{S16}$$

The output state after the WGA is

$$|\psi_{\text{out}}\rangle = \left(V_{11}a_1^\dagger + V_{12}a_2^\dagger + V_{13}a_3^\dagger\right)\left(V_{21}a_1^\dagger + V_{22}a_2^\dagger + V_{23}a_3^\dagger\right)\left(V_{31}a_1^\dagger + V_{32}a_2^\dagger + V_{33}a_3^\dagger\right)|0\rangle_1 |0\rangle_2 |0\rangle_3 . \tag{S17}$$

The three-photon HOM effect is obtained when the probability of finding the output state $|1\rangle_1 |1\rangle_2 |1\rangle_3$ is zero, i.e.,

$$V_{11}V_{22}V_{33} + V_{12}V_{23}V_{31} + V_{13}V_{21}V_{32} + V_{11}V_{23}V_{32} + V_{12}V_{21}V_{33} + V_{13}V_{22}V_{31} = 0. \tag{S18}$$

We thus have [cf. Eq. (S14)]

$$\cos^4\left(\frac{G}{2}\right)(3\cos G - 2) - (3\cos G + 2)\cos(4\theta)\sin^4\left(\frac{G}{2}\right) = 0. \tag{S19}$$

The solutions to Eq. (S19) are shown in Fig. 1. For $G = \frac{\pi}{2}$ and $\theta = \frac{\pi}{4}$, then

$$V = \begin{pmatrix} \frac{1}{2} & \frac{i}{\sqrt{2}} & -\frac{1}{2} \\ \frac{i}{\sqrt{2}} & 0 & \frac{i}{\sqrt{2}} \\ -\frac{1}{2} & \frac{i}{\sqrt{2}} & \frac{1}{2} \end{pmatrix}. \tag{S20}$$

This will transform the input modes as

$$a_1^\dagger \to \frac{1}{2}a_1^\dagger + \frac{i}{\sqrt{2}}a_2^\dagger - \frac{1}{2}a_3^\dagger, \tag{S21}$$

$$a_2^\dagger \to \frac{i}{\sqrt{2}}a_1^\dagger + \frac{i}{\sqrt{2}}a_3^\dagger, \tag{S22}$$

$$a_3^\dagger \to -\frac{1}{2}a_1^\dagger + \frac{i}{\sqrt{2}}a_2^\dagger + \frac{1}{2}a_3^\dagger. \tag{S23}$$

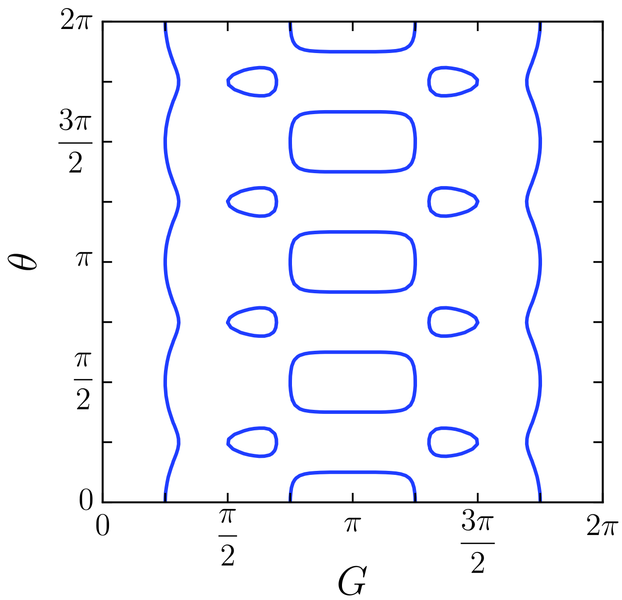

Fig. S 1. Solutions to Eq. (S19).

S3. PUMP-PROBE SPECTROSCOPY WITH THREE ENTANGLED PHOTONS

A. Derivation of the frequency-dispersed photon-counting signal Eq. (7)

Starting from the definition of signal Eq. (5) and using Eq. (6), we have

$$
\begin{aligned}
S(\omega_2,\omega_3;\Gamma) =& \left\langle a_3^\dagger(\omega_3)a_2^\dagger(\omega_2)a_2(\omega_2)a_3(\omega_3)\right\rangle && \text{(S24)}\\
=&\mathrm{tr}\left[a_3^\dagger(\omega_3)a_2^\dagger(\omega_2)a_2(\omega_2)a_3(\omega_3)\rho_I(t\to\infty)\right] && \text{(S25)}\\
=&S_0-\frac{i}{\hbar}\mathscr{T}\int_{-\infty}^{\infty}dt\,\mathrm{tr}\left[a_3^\dagger(\omega_3)a_2^\dagger(\omega_2)a_3(\omega_3)a_2(\omega_2)H_{\mathrm{int},-}(t)\rho_{\mathrm{int}}(t)\right]. && \text{(S26)}
\end{aligned}
$$

In Eq. (S26), the first term S_0 describes the expectation value in the absence of any interaction with the system and thus can be subtracted. The signal can be written as [7]

$$
\begin{aligned}
S(\omega_2,\omega_3;\Gamma) =& -\frac{i}{\hbar}\mathscr{T}\int_{-\infty}^{\infty}dt\,\mathrm{tr}\left[[a_3^\dagger(\omega_3)a_2^\dagger(\omega_2)a_3(\omega_3)a_2(\omega_2),H_{\mathrm{int}}(t)]\rho_{\mathrm{int}}(t)\right] && \text{(S27)}\\
=&\frac{1}{\pi\hbar}\mathscr{T}\Im\int_{-\infty}^{\infty}dt\,e^{i\omega_2 t}\left\langle a_3^\dagger(\omega_3)a_3(\omega_3)E_2^\dagger(\omega_2)V(t)\right\rangle, && \text{(S28)}
\end{aligned}
$$

where the commutator in Eq. (S27) is evaluated to

$$
\begin{aligned}
&[a_3^\dagger(\omega_3)a_2^\dagger(\omega_2)a_3(\omega_3)a_2(\omega_2),H_{\mathrm{int}}(t)] && \text{(S29)}\\
=&a_3^\dagger(\omega_3)a_3(\omega_3)\int\frac{dt_a}{2\pi}\int\frac{dt_b}{2\pi}e^{i\omega_2(t_b-t_a)}[a_2^\dagger(t_a)a_2(t_b),E_2^\dagger(t)V(t)+E_2(t)V^\dagger(t)] && \text{(S30)}\\
=&\frac{1}{2\pi}a_3^\dagger(\omega_3)a_3(\omega_3)[E_2^\dagger(\omega_2)V(t)e^{i\omega_2 t}-E_2(\omega_2)V^\dagger(t)e^{-i\omega_2 t}]. && \text{(S31)}
\end{aligned}
$$

B. Two-photon absorption with three entangled photons

The contributions of diagrams (I) and (II) to Eq. (8) where all interactions are on the ket are

$$
\begin{aligned}
& S^{(\mathrm{I})}(\omega_2,\omega_3;\Gamma)+S^{(\mathrm{II})}(\omega_2,\omega_3;\Gamma) && \text{(S32)}\\
=&\frac{\omega_{10}\omega_{20}}{\pi\hbar}\left(\frac{\hbar}{4\pi\varepsilon_0 cA}\right)^2\Im\left(\frac{-i}{\hbar}\right)^3\int_{-\infty}^{\infty}dt\int_{-\infty}^{t}d\tau_3\int_{-\infty}^{\tau_3}d\tau_2\int_{-\infty}^{\tau_2}d\tau_1\, e^{i\omega_2 t}\left\langle V(t)V(\tau_3)V^\dagger(\tau_2)V^\dagger(\tau_1)\right\rangle\\
&\left[\left\langle a_3^\dagger(\omega_3)a_3(\omega_3)a_2^\dagger(\omega_2)a_1^\dagger(\tau_3)a_2(\tau_2)a_1(\tau_1)\right\rangle+\left\langle a_3^\dagger(\omega_3)a_3(\omega_3)a_2^\dagger(\omega_2)a_1^\dagger(\tau_3)a_1(\tau_2)a_2(\tau_1)\right\rangle\right] && \text{(S33)}\\
=&\frac{\omega_{10}\omega_{20}}{\pi\hbar}\left(\frac{\hbar}{4\pi\varepsilon_0 cA}\right)^2\Im\left(\frac{-i}{\hbar}\right)^3\int_{-\infty}^{\infty}dt\int_{-\infty}^{t}d\tau_3\int_{-\infty}^{\tau_3}d\tau_2\int_{-\infty}^{\tau_2}d\tau_1\int d\omega_a\int d\omega_b\int d\omega_c\\
&e^{i\omega_a\tau_3}e^{-i\omega_b\tau_2}e^{-i\omega_c\tau_1}e^{i\omega_2 t}\left\langle V(t)V(\tau_3)V^\dagger(\tau_2)V^\dagger(\tau_1)\right\rangle\\
&\left[\left\langle a_3^\dagger(\omega_3)a_2^\dagger(\omega_2)a_1^\dagger(\omega_a)a_3(\omega_3)a_2(\omega_b)a_1(\omega_c)\right\rangle+\left\langle a_3^\dagger(\omega_3)a_2^\dagger(\omega_2)a_1^\dagger(\omega_a)a_3(\omega_3)a_2(\omega_c)a_1(\omega_b)\right\rangle\right]. && \text{(S34)}
\end{aligned}
$$

The contributions of diagrams (III) and (IV) to Eq. (8) with three interactions on the ket and one on the bra are

$$
\begin{aligned}
& S^{(\mathrm{III})}(\omega_2,\omega_3;\Gamma)+S^{(\mathrm{IV})}(\omega_2,\omega_3;\Gamma) && \text{(S35)}\\
=&-\frac{\omega_{10}\omega_{20}}{\pi\hbar}\left(\frac{\hbar}{4\pi\varepsilon_0 cA}\right)^2\Im\left(\frac{-i}{\hbar}\right)^3\int_{-\infty}^{\infty}dt\int_{-\infty}^{t}d\tau_3\int_{-\infty}^{t}d\tau_2\int_{-\infty}^{\tau_2}d\tau_1\, e^{i\omega_2 t}\left\langle V(\tau_3)V(t)V^\dagger(\tau_2)V^\dagger(\tau_1)\right\rangle\\
&\left[\left\langle a_1^\dagger(\tau_3)a_3^\dagger(\omega_3)a_3(\omega_3)a_2^\dagger(\omega_2)a_2(\tau_2)a_1(\tau_1)\right\rangle+\left\langle a_1^\dagger(\tau_3)a_3^\dagger(\omega_3)a_3(\omega_3)a_2^\dagger(\omega_2)a_1(\tau_2)a_2(\tau_1)\right\rangle\right] && \text{(S36)}\\
=&-\frac{\omega_{10}\omega_{20}}{\pi\hbar}\left(\frac{\hbar}{4\pi\varepsilon_0 cA}\right)^2\Im\left(\frac{-i}{\hbar}\right)^3\int_{-\infty}^{\infty}dt\int_{-\infty}^{t}d\tau_3\int_{-\infty}^{t}d\tau_2\int_{-\infty}^{\tau_2}d\tau_1\int d\omega_a\int d\omega_b\int d\omega_c\\
&e^{i\omega_a\tau_3}e^{-i\omega_b\tau_2}e^{-i\omega_c\tau_1}e^{i\omega_2 t}\left\langle V(\tau_3)V(t)V^\dagger(\tau_2)V^\dagger(\tau_1)\right\rangle\\
&\left[\left\langle a_3^\dagger(\omega_3)a_2^\dagger(\omega_2)a_1^\dagger(\omega_a)a_3(\omega_3)a_2(\omega_b)a_1(\omega_c)\right\rangle+\left\langle a_3^\dagger(\omega_3)a_2^\dagger(\omega_2)a_1^\dagger(\omega_a)a_3(\omega_3)a_2(\omega_c)a_1(\omega_b)\right\rangle\right]. && \text{(S37)}
\end{aligned}
$$

The field correlation functions for the TPA signals are of the form $\left\langle a_3^\dagger a_2^\dagger a_1^\dagger a_3 a_2 a_1 \right\rangle$, and can be expressed as

$$\left\langle a_3^\dagger(\omega_3) a_2^\dagger(\omega_2) a_1^\dagger(\omega_a) a_3(\omega_3) a_2(\omega_b) a_1(\omega_c) \right\rangle \tag{S38}$$

$$\begin{aligned}
=&[c_{31}c_{22}c_{13}F^*(\omega_3,\omega_2,\omega_a)+c_{31}c_{23}c_{12}F^*(\omega_3,\omega_a,\omega_2)+c_{32}c_{21}c_{13}F^*(\omega_2,\omega_3,\omega_a)\\
&+c_{32}c_{23}c_{11}F^*(\omega_a,\omega_3,\omega_2)+c_{33}c_{21}c_{12}F^*(\omega_2,\omega_a,\omega_3)+c_{33}c_{22}c_{11}F^*(\omega_a,\omega_2,\omega_3)]\\
&[c_{31}^*c_{22}^*c_{13}^*F(\omega_3,\omega_b,\omega_c)+c_{31}^*c_{23}^*c_{12}^*F(\omega_3,\omega_c,\omega_b)+c_{32}^*c_{21}^*c_{13}^*F(\omega_b,\omega_3,\omega_c)\\
&+c_{32}^*c_{23}^*c_{11}^*F(\omega_c,\omega_3,\omega_b)+c_{33}^*c_{21}^*c_{12}^*F(\omega_b,\omega_c,\omega_3)+c_{33}^*c_{22}^*c_{11}^*F(\omega_c,\omega_b,\omega_3)],
\end{aligned} \tag{S39}$$

where c_{ij} is the matrix element of the transformation matrix C, and $F(\omega_a,\omega_2,\omega_3)$ is the spectral amplitude given by Eq. (2) of the main text.

S4. PUMP-PROBE SPECTROSCOPY WITH ENTANGLED PHOTON-PAIR

A. Transformation matrix for the Mach-Zehnder interferometer

The Mach-Zehnder interferometer for the pump-probe experiment with entangled photon-pair consists of two 50:50 beam splitters (BS's). The transformation matrix for the BS is [8]

$$M = \begin{pmatrix} \frac{1}{\sqrt{2}} & \frac{i}{\sqrt{2}} \\ \frac{i}{\sqrt{2}} & \frac{1}{\sqrt{2}} \end{pmatrix}. \tag{S40}$$

The transformation matrix for the MZI is

$$C = M^\dagger \,\mathrm{diag}(e^{i\phi},1)\, M, \tag{S41}$$

which will transform

$$a_1^\dagger \to c_{11}a_1^\dagger + c_{12}a_2^\dagger, \tag{S42}$$
$$a_2^\dagger \to c_{21}a_1^\dagger + c_{22}a_2^\dagger. \tag{S43}$$

B. Two-photon absorption with entangled photon-pair

The signal is detected by spectrally dispersing the probe photon a_2 [see Fig. 2(c)]. Similar to the derivation of Eq. (S28), we obtain the expression for the signal with two entangled photons:

$$S^{(2\mathrm{p})} = \left\langle a_2^\dagger(\omega_2) a_2(\omega_2) \right\rangle \tag{S44}$$
$$= \frac{1}{\pi\hbar}\Im\mathscr{T}\int_{-\infty}^{\infty} dt\,\mathrm{tr}\left[E_2^\dagger(\omega_2)e^{i\omega_2 t}V(t)\rho_{\mathrm{int}}(t)\right]. \tag{S45}$$

Expanding the density matrix $\rho_{\mathrm{int}}(t)$ to second order in E_1 and first order in E_2, we obtain same diagrams as those in Fig. 3.

The contributions of diagrams (I) and (II) to $S^{(2p)}_{\rm TPA}$ are

$$
\begin{aligned}
&S^{(\mathrm{I})}(\omega_{p0},\omega_2;\Gamma)+S^{(\mathrm{II})}(\omega_{p0},\omega_2;\Gamma) &\text{(S46)}\\
=&\frac{\omega_{10}\omega_{20}}{\pi\hbar}\left(\frac{\hbar}{4\pi\varepsilon_0 cA}\right)^2\Im\left(\frac{-i}{\hbar}\right)^3\int_{-\infty}^{\infty}dt\int_{-\infty}^{t}d\tau_3\int_{-\infty}^{\tau_3}d\tau_2\int_{-\infty}^{\tau_2}d\tau_1\, e^{i\omega_2 t}\left\langle V(t)V(\tau_3)V^\dagger(\tau_2)V^\dagger(\tau_1)\right\rangle\\
&\left[\left\langle a_2^\dagger(\omega_2)a_1^\dagger(\tau_3)a_2(\tau_2)a_1(\tau_1)\right\rangle+\left\langle a_2^\dagger(\omega_2)a_1^\dagger(\tau_3)a_1(\tau_2)a_2(\tau_1)\right\rangle\right] &\text{(S47)}\\
=&\frac{\omega_{10}\omega_{20}}{\pi\hbar}\left(\frac{\hbar}{4\pi\varepsilon_0 cA}\right)^2\Im\left(\frac{-i}{\hbar}\right)^3\int_{-\infty}^{\infty}dt\int_{-\infty}^{t}d\tau_3\int_{-\infty}^{\tau_3}d\tau_2\int_{-\infty}^{\tau_2}d\tau_1\int d\omega_a\int d\omega_b\int d\omega_c\\
&e^{i\omega_a\tau_3}e^{-i\omega_b\tau_2}e^{-i\omega_c\tau_1}e^{i\omega_2 t}\left[\left\langle a_2^\dagger(\omega_2)a_1^\dagger(\omega_a)a_2(\omega_b)a_1(\omega_c)\right\rangle+\left\langle a_2^\dagger(\omega_2)a_1^\dagger(\omega_a)a_2(\omega_c)a_1(\omega_b)\right\rangle\right]\\
&\left\langle V(t)V(\tau_3)V^\dagger(\tau_2)V^\dagger(\tau_1)\right\rangle. &\text{(S48)}
\end{aligned}
$$

The contributions of diagrams (III) and (IV) to $S^{(2p)}_{\rm TPA}$ are

$$
\begin{aligned}
&S^{(\mathrm{III})}(\omega_{p0},\omega_2;\Gamma)+S^{(\mathrm{IV})}(\omega_{p0},\omega_2;\Gamma) &\text{(S49)}\\
=&-\frac{\omega_{10}\omega_{20}}{\pi\hbar}\left(\frac{\hbar}{4\pi\varepsilon_0 cA}\right)^2\Im\left(\frac{-i}{\hbar}\right)^3\int_{-\infty}^{\infty}dt\int_{-\infty}^{t}d\tau_3\int_{-\infty}^{t}d\tau_2\int_{-\infty}^{\tau_2}d\tau_1\, e^{i\omega_2 t}\left\langle V(\tau_3)V(t)V^\dagger(\tau_2)V^\dagger(\tau_1)\right\rangle\\
&\left[\left\langle a_1^\dagger(\tau_3)a_2^\dagger(\omega_2)a_2(\tau_2)a_1(\tau_1)\right\rangle+\left\langle a_1^\dagger(\tau_3)a_2^\dagger(\omega_2)a_1(\tau_2)a_2(\tau_1)\right\rangle\right] &\text{(S50)}\\
=&-\frac{\omega_{10}\omega_{20}}{\pi\hbar}\left(\frac{\hbar}{4\pi\varepsilon_0 cA}\right)^2\Im\left(\frac{-i}{\hbar}\right)^3\int_{-\infty}^{\infty}dt\int_{-\infty}^{t}d\tau_3\int_{-\infty}^{t}d\tau_2\int_{-\infty}^{\tau_2}d\tau_1\int d\omega_a\int d\omega_b\int d\omega_c\\
&e^{i\omega_a\tau_3}e^{-i\omega_b\tau_2}e^{-i\omega_c\tau_1}e^{i\omega_2 t}\left[\left\langle a_2^\dagger(\omega_2)a_1^\dagger(\omega_a)a_2(\omega_b)a_1(\omega_c)\right\rangle+\left\langle a_2^\dagger(\omega_2)a_1^\dagger(\omega_a)a_2(\omega_c)a_1(\omega_b)\right\rangle\right]\\
&\left\langle V(\tau_3)V(t)V^\dagger(\tau_2)V^\dagger(\tau_1)\right\rangle. &\text{(S51)}
\end{aligned}
$$

The normally-ordered four-point field correlation function is

$$
\begin{aligned}
&\left\langle a_2^\dagger(\omega_2)a_1^\dagger(\omega_a)a_2(\omega_b)a_1(\omega_c)\right\rangle &\text{(S52)}\\
=&|c_{21}|^2|c_{12}|^2F^*(\omega_2,\omega_a)F(\omega_b,\omega_c)+c_{21}c_{12}c_{22}^*c_{11}^*F^*(\omega_2,\omega_a)F(\omega_c,\omega_b)\\
&+c_{22}c_{11}c_{21}^*c_{12}^*F^*(\omega_a,\omega_2)F(\omega_b,\omega_c)+|c_{22}|^2|c_{11}|^2F^*(\omega_a,\omega_2)F(\omega_c,\omega_b). &\text{(S53)}
\end{aligned}
$$

Here the two-photon amplitude is [9]

$$
F(\omega_1,\omega_2)=\sqrt{\frac{|T_{p1}-T_{p2}|}{\pi\sigma_p}}(2\gamma)^{1/4}e^{-\frac{(\omega_1+\omega_2-\omega_{p0})^2}{2\sigma_p^2}}e^{-\gamma[T_{p1}(\omega_1-\omega_{10})+T_{p2}(\omega_2-\omega_{20})]^2}, \tag{S54}
$$

where σ_p is the pump bandwidth, $\omega_{\mu0}$ ($\mu=p$, 1 and 2) is the central frequency of pulse μ, $\gamma=0.0482304$, and the two time delays are defined similarly to those in Eq. (2) of the main text.

[1] Q.-Y. Zhang, G.-T. Xue, P. Xu, Y.-X. Gong, Z. Xie, and S. Zhu, Phys. Rev. A **97**, 022327 (2018).

[2] L. K. Shalm, D. R. Hamel, Z. Yan, C. Simon, K. J. Resch, and T. Jennewein, Nat. Phys. **9**, 19 (2013).

[3] W. P. Grice, A. B. U'Ren, and I. A. Walmsley, Phys. Rev. A **64**, 063815 (2001).

[4] M. V. Fedorov, Y. M. Mikhailova, and P. A. Volkov, J. Phys. B: At. Mol. Opt. Phys. **42**, 175503 (2009).

[5] S. Mährlein, J. Von Zanthier, and G. S. Agarwal, Opt. Express **23**, 15833 (2015).

[6] K. Suzuki, V. Sharma, J. G. Fujimoto, E. P. Ippen, and Y. Nasu, Opt. Express **14**, 2335 (2006).

[7] F. Schlawin, K. E. Dorfman, and S. Mukamel, Phys. Rev. A **93**, 023807 (2016).

[8] O. Roslyak, C. A. Marx, and S. Mukamel, Phys. Rev. A **79**, 033832 (2009).

[9] K. E. Dorfman, F. Schlawin, and S. Mukamel, Rev. Mod. Phys. **88**, 045008 (2016).